CHEMISTRY
A European Journal

A Journal of
ChemPubSoc Europe

Accepted Article

Title: Versatile and homogeneous DNA tetraplex platform for constructing label-free logic devices: from design to application

Authors: Dan Huang, Chunrong Yang, Ye Yao, Jicheng Li, Chen Guo, Jianchi Chen, Yi Zhang, Shu Yang, Qianfan Yang, and Yalin Tang

To be cited as: *Chem. Eur. J.* 10.1002/chem.201900734

Link to VoR: http://dx.doi.org/10.1002/chem.201900734

Supported by
ACES

WILEY-VCH

10.1002/chem.201900734

WILEY-VCH

FULL PAPER

Versatile and homogeneous DNA tetraplex platform for constructing label-free logic devices: from design to application

Dan Huang,[a] Chunrong Yang,[a] Ye Yao,[a] Jicheng Li, [a] Chen Guo,[a] Jianchi Chen,[a] Yi Zhang,[b] Shu Yang,[b] Qianfan Yang,*[a] Yalin Tang[c]

Abstract: The design of DNA-based logic circuits has become an active research field in DNA nanotechnology and holds great potential in intelligent bioanalysis. To date, although many DNA-based logic systems have been realized, the implementation of advanced logic functions is still challenging, especially with simple and homogeneous composition. In this work, by integrating two DNA tetraplex structures (G-quadruplex and i-motif) together, a completely label-free logic platform with highly scalability was established, on which a series of advanced functions were realized, including arithmetic (the adders and subtractors) and non-arithmetic ones (the majority and dual-transfer gates). Further, the platform was also applied as an intelligent biosensor to co-analyse two cancer-related micro-RNAs with high sensitivities and specificities. Considering the excellent versatility, expandability and biocompatibility, the platform may promote the development of DNA computing and hold great potential in multi-parameter sensing and medical diagnosis.

Introduction

Molecular computing, especially DNA computing, paves a new avenue for an alternative approach to silicon-based circuits due to its potential advantages in circumventing the limitation of miniaturization.[1] Since the first example of DNA computation solved the seven-city Hamiltonian path problem,[2] numerous DNA-based intelligent systems have been designed, implementing both arithmetic (such as Boolean logic gate[3], half/full adder and half/full subtractor)[4] and non-arithmetic (such as encoders/decoders,[5] multiplexers/demultiplexers[6], keypad lock[7] and majority gate[8]) functions. Among these systems, universal platforms that are capable of executing multifarious logic operations are particularly attractive as they can process information comprehensively and more efficiently.[9]

[a] D. Huang, C.R. Yang, Y. Yao, J.C. Li, C. Guo, J.C. Chen, Dr. Q.F. Yang
College of Chemistry, Sichuan University
Chengdu 610064 (P. R. China)
E-mail: yangqf@scu.edu.cn
[b] Y Zhang, Dr. S. Yang
Department West China School of Pharmacy, Sichuan University
Chengdu 610064 (P. R. China)
[c] Prof. Yalin Tang
National Laboratory for Molecular Sciences, Centre for Molecular Sciences, State Key Laboratory for Structural Chemistry of Unstable and Stable Species, Institute of Chemistry, Chinese Academy of Sciences
Beijing, 100190 (P. R. China)
Supporting information for this article is given via a link at the end of the document.

To date, several DNA-based logic platforms with excellent performances have been designed.[10] Due to the structural polymorphism, non-covalent probes and critical roles in biological regulation, G-quadruplex structure is an ideal building block for constructing DNA logics. Based on the winding and unwinding of certain G-quadruplexes, several platforms have been developed to implement a series of Boolean logic gate functions.[9a, 11] However, the G-quadruplexes can produce only single output. To implement advanced logic operations, other signal transducers (like double-labelled molecular beacon[12]) have to be introduced. As a result, most of the reported DNA logic platforms cannot totally get rid of pre-labelled components, resulting in complicated modification process and increased operating time/costs. Most recently, DNA-templated nanoclusters (like AgNCs and CuNPs) provide another kind of label-free signal producing mode and some logic circuits (such as multiplexers/demultiplexers, half adders/subtractors) have been designed by combining the nanoclusters with G-quadruplex probes.[13] These works greatly improve the development of DNA computing, however, designing a completely label-free and homogeneous logic platform that can implement diverse advanced logic functions is still challenging, especially with simple composition.

Apart from G-quadruplexes folded by Guanine (G)-rich strands, [14] i-motifs folded by Cytosine (C)-rich ones are another kind of DNA tetraplex structure. Owing to the structural stability, potential physiological functions, and non-covalent probes, i-motifs have gained increasing attention and been involved in the construction of basic Boolean logic gates.[15] Since G- and C-rich strands can complement with each other, integrating G-quadruplex and i-motif in one circuit can not only make the best of DNA material but also pave an access to construct a completely label-free and homogeneous platform. However, logic circuit based on the both DNA tetraplexes has not been reported so far. One of the crucial reasons is that i-motif ligands usually show poor specificity. For example, the common ligands for i-motif, including crystal violet,[16] berberine[17] and quinaldine red,[18] cannot identify i-motif from double-stranded DNA or G-quadruplex, which are incapable of producing independent signal in coexistence with G-quadruplexes.

In this work, we integrated G-quadruplex and i-motif together and successfully developed a versatile and homogeneous DNA logic platform. On which, various advanced molecular circuits, including the majority gate, half/full adder, full subtractor and dual-transfer gate, were constructed with completely label-free signals and homogeneous components. To demonstrate the enormous potential of the platform in practice, the platform was further applied to co-analyze two cancer-associated micro-RNAs (miRNA) as an intelligent biosensor.

10.1002/chem.201900734

Results and Discussion

The foundational design of the DNA tetraplex platform

As shown in Scheme 1A, a pair of strands with G-rich or C-rich segment were designed as the core components of the platform. They can separately fold into intermolecular G-quadruplex or i-motif in weak acidic potassium buffer (10 mM K_2HPO_4/ KH_2PO_4, 100 mM KCl, 10 mM $MgCl_2$, pH=5.5, termed PBS). Due to the complementarity, the two strands can hybridize with each other spontaneously when coexisting. Two fluorescence probes, ***Nap-s*** [3,3'-di(3-sulfopropyl)-4,5,4',5'-dibenzo-9-methylthiacarbocyanine-triethyl-ammonium salt] and ***Ben-eth*** [2,2'-diethyl-9-methylselena-carbocyanine bromide] (the molecular formulas were shown in Scheme 1B), were employed to produce the detectable signals. ***Nap-s*** is a typical cyanine dye with extended plane conjugated system, which could bind on the terminal G-quartet of G-quadruplex through π-π stacking interaction. Our previous work has proven that ***Nap-s*** and its analogues have weak fluorescence signal. And they could specifically recognize G-quadruplex by end-stacking model and generated an obvious enhancement of fluorescence signal at 613nm. [19] Compared with G-quadruplex, i-motif has smaller planar structure, and thus probes with large planar aromatic structures are unsuitable. On the contrary, ***Ben-eth*** has narrow aromatic rings and has been verified to specifically insert into the groove of i-motif to recognize i-motif formation, presenting a strong fluorescence signal at 583 nm. [15a] As shown in Scheme 1C-D, in PBS, ***Nap-s*** presents strong fluorescence signal at 613 nm with the G-rich strand while undetectable signal with the C-rich one (blue curves), and ***Ben-eth*** presents an opposite signal pattern: strong fluorescence at 583 nm with the C-rich strand while weak signal with the G- rich one (red curves). Further, we have characterized the effect of dyes on DNA tetraplexes using CD, the results showed that the addition of dyes has little effect on G-quadruplex and i-motif structures (Figure S16). The unique and distinguishable spectral properties regarding certain tetraplex structures make the two probes excellent compatible signal transducers for dual-output logic circuits.

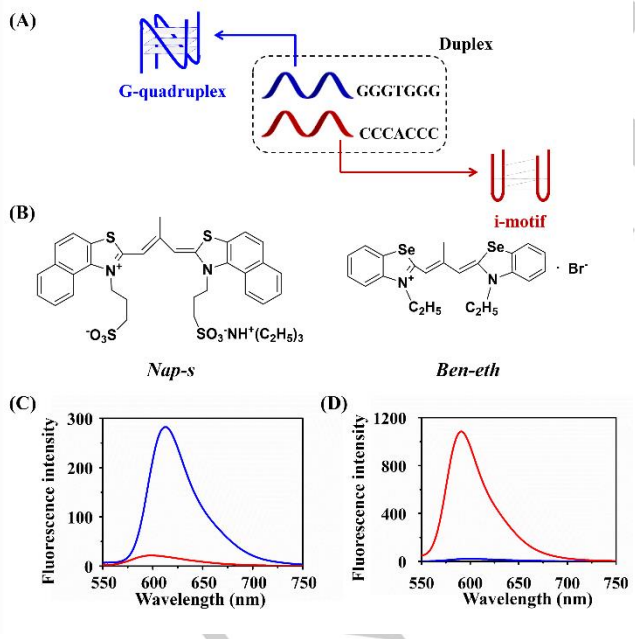

Scheme 1. (A) The core sequences and tetraplex structures for the platform. (B) The molecular formulas of the two specific probes, i.e. ***Nap-s*** and ***Ben-eth***. The fluorescence spectra of ***Nap-s*** (blue curves) and ***Ben-eth*** (red curves) with the G-rich (C) and C-rich strand (D) in PBS.

To realize the desired functions, the presence and absence of the inputs were defined as "1" and "0", respectively. And the normalized changes of the fluorescence intensities were defined as the binary output signals: higher than the threshold (set as 0.4) were considered as "1", otherwise as "0". The definition suits for all the circuits in this work.

The construction of the majority logic gate based on i-motif structure

In electronic circuits, the function of a voting counter is implemented by the majority gate (Figure 1B), which returns Approval (TRUE) result only when more than half of its inputs (voters) are Approval (TURE). As shown in Figure 1B, it is composed of a switchable AND/OR gate, which can be served as a basic component of advanced logic devices and plays important roles in the computing field and multi-target diagnosis.[20] Herein, a three-input majority gate was firstly designed on i-motif structure. According to the desired function, the normalized enhancement of ***Ben-eth*** fluorescence intensity (F_x/F_{max}) was considered as the voting output signal, where F_{max} is the strongest fluorescence intensity of ***Ben-eth*** in all inputting situations and F_x is that in each case.

As depicted schematically in Figure 1A, a G-rich strand **Init** in PBS was designed as the initial state, and **IN1**, **IN2** and **IN3** as the three voters (inputs) (all sequences were listed in Table S1). Each input strand is composed of a C-rich region (red wavy line) and two flanking regions (blue, yellow or green wavy lines). The C-rich regions can either complement with **Init** or form intermolecular i-motifs with each other, and the flanking ones can complement with other inputs in pairs. The flanking regions are designed to be longer than the C-rich sequence, so that **IN1**, **IN2,** and **IN3** prefer hybridizing with each other to complementing with **Init**.

As shown in Figure 1D, in no Approval (no input) case, there was no ***Ben-eth*** fluorescence (black curve). When only one voter approved, **Init** would complement with **IN1**, **IN2** or **IN3** to form stable duplexes, presenting weak ***Ben-eth*** fluorescence signals (red, light blue or green curve). When two or more voters passed, the input strands tended to complement with each other and to form heterogeneous i-motifs, resulting in an obvious enhancement of ***Ben-eth*** signal (pink, purple, mazarine or orange curve). The histograms of normalized outputs were plotted in Figure 1E, and the obtained truth table (Figure 1C) was consistent with the majority gate. The states and structures of all the DNA strands in various voting situations were confirmed by native polyacrylamide gel electrophoresis (PAGE) and circular dichroism (CD) (Figure S9).

10.1002/chem.201900734

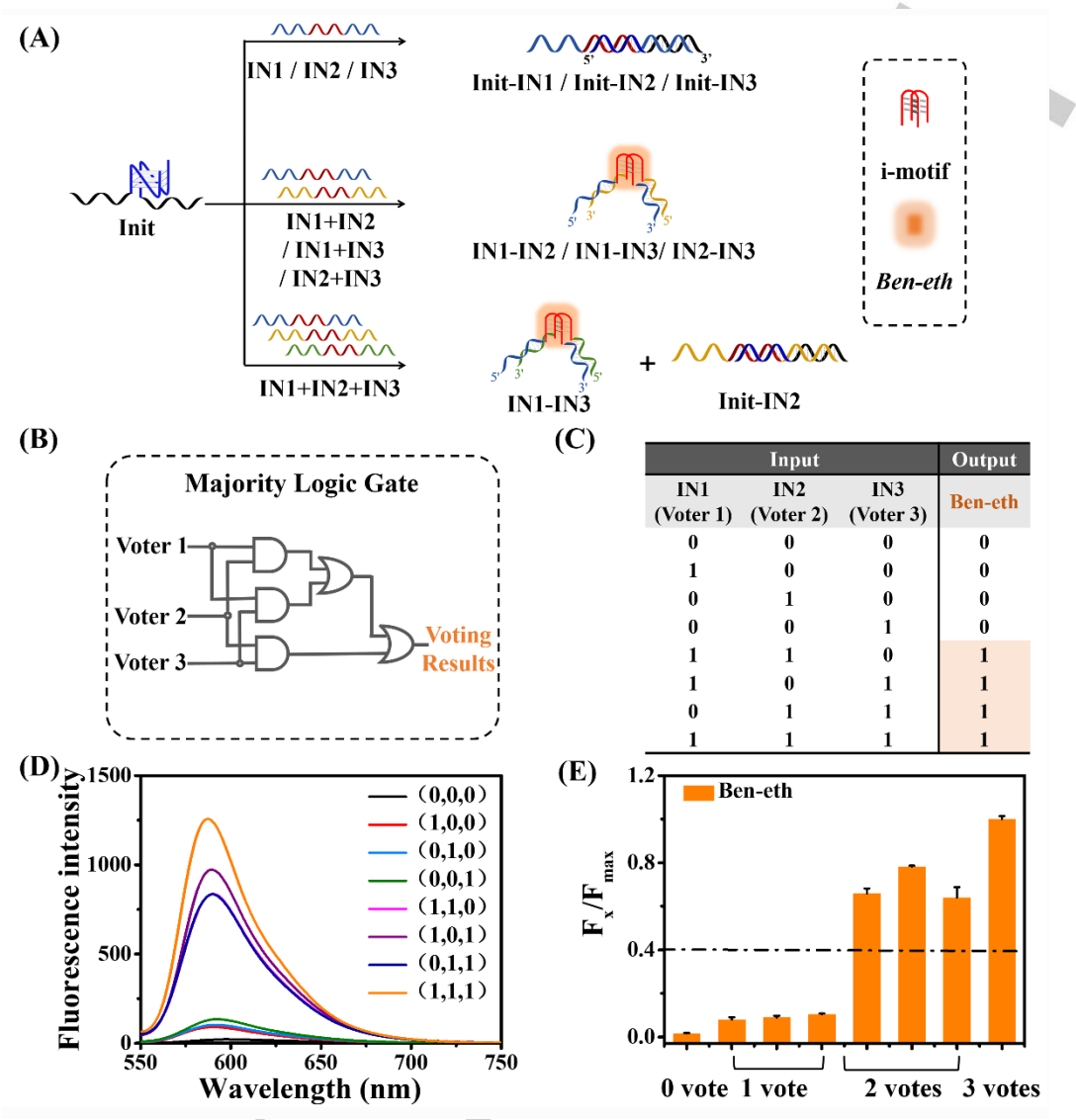

Figure 1. The majority gate. (A) The schematic diagram of the majority gate based on i-motif structure. The logic circuit (B) and the truth table (C) of the majority gate. (D) The fluorescence spectra of ***Ben-eth*** in various input situations. (E) The column diagram of the normalized output signals.

The construction of the adders and subtractors by integrating G-quadruplex and i-motif together

In electronic computer, the arithmetic operations are essential for data and information processing and the most fundamental one implemented by adder. The simplest adder circuit is the half adder, which is composed of parallel AND and XOR logic gates to generate two output channels, CARRY (C_i) and SUM (S) (Figure 2B).[4a] Based on the majority gate, a half adder was designed by employing both i-motif and G-quadruplex.

As shown in Figure 2A, **Init**, **IN1** (addend) and **IN2** (augend) are all the same as those in the majority gate. In PBS, **Init** strand in the initial state could form bimolecular G-quadruplexes and give rise to high ***Nap-s*** fluorescence specifically. To achieve the desired function, the normalized change of ***Nap-s*** fluorescence [(F_{max} -F_x)/F_{max}] was defined as the S output and normalized enhancement (F_x/F_{max}) of ***Ben-eth*** was defined as the C_i output of the half adder.

As shown in Figure 2E-F, when the addend and augend were "0", the system only contains **Init** G-quadruplex, thus the ***Ben-eth*** signal was not enhanced while the signal of ***Nap-s*** was lightened up, indicating C_i = 0 and S = 0. In the case that either the addend or augend was "1", namely inputting **IN1** or **IN2**, **Init-IN1** or **Init-IN2** duplex was formed d the consequential weak fluorescence of both ***Ben-eth*** and ***Nap-s*** indicated the result of C_i = 0 and S = 1. In the case that both the addend and augend were "1", heterogeneous i-motif of **IN1-IN2** was formed due to the longer complementary regions, and the **Init** G-quadruplex was released.

In this case, both ***Ben-eth*** and ***Nap-s*** signals were enhanced, presenting C_i = 1 and S = 0. The normalized outputs were plotted as histogram in Figure 2D, which was consistent with the truth table (Figure 2C) of the half adder. The states and structures of all the DNA strands in various situations were confirmed by CD (Figure S9) and PAGE (Figure S10).

Although the half adder can process the addition of two binary numbers at the current bit, it is difficult to process continuous addition. To solve this problem, the full adder, which could consider the low carry (C_{i-1}) from the previous addition, was further introduced. A full adder consists of two half adders and an OR gate to perform C_i and S digits (Figure 3B). So far, only three examples of DNA-based full adders have been experimentally constructed and none of them are completely label-free.[4a, 12, 21] Herein, we realized a completely label-free full adder for the first time based on the tetraplex platform.

As shown in Figure 3A, **Init** and the three inputs [**IN1** (addend), **IN2** (augend) and **IN3** (low-bit carry C_{i-1})] are identical with those in the majority gate and the half adder. For the full adder (Figure 3E-F), the operations when C_{i-1} = "0" are similar to those of the half adder. In the case of C_{i-1} = "1", i.e. inputting **IN3**, when the addend and augend were "0", **Init** and **IN3** prefer to form stable duplex. The weak fluorescence of both ***Ben-eth*** and ***Nap-s*** presents C_i= 0 and S = 1. When either the addend or augend was "1", the **IN1/IN3** or **IN2/IN3** preferred to form the duplex with heterogeneous i-motif, leaving the **Init** G-quadruplex alone. In this case, the strong signals of both ***Ben-eth*** and ***Nap-s*** were obtained, presenting C_i = 1 and S = 0. When the addend and augend were both "1", **IN1** and IN3 had the stronger affinity to form i-motif and the **Init** G-quadruplex was suppressed by **IN2** definitions are opposite in the ***Ben-eth*** and ***Nap-s*** channels: the high ("light-up") fluorescence intensity of ***Ben-eth*** was assigned as "1", while that of ***Nap-s*** was assigned as "0". To further simplify the processing of output signals, a dual-transfer gate was

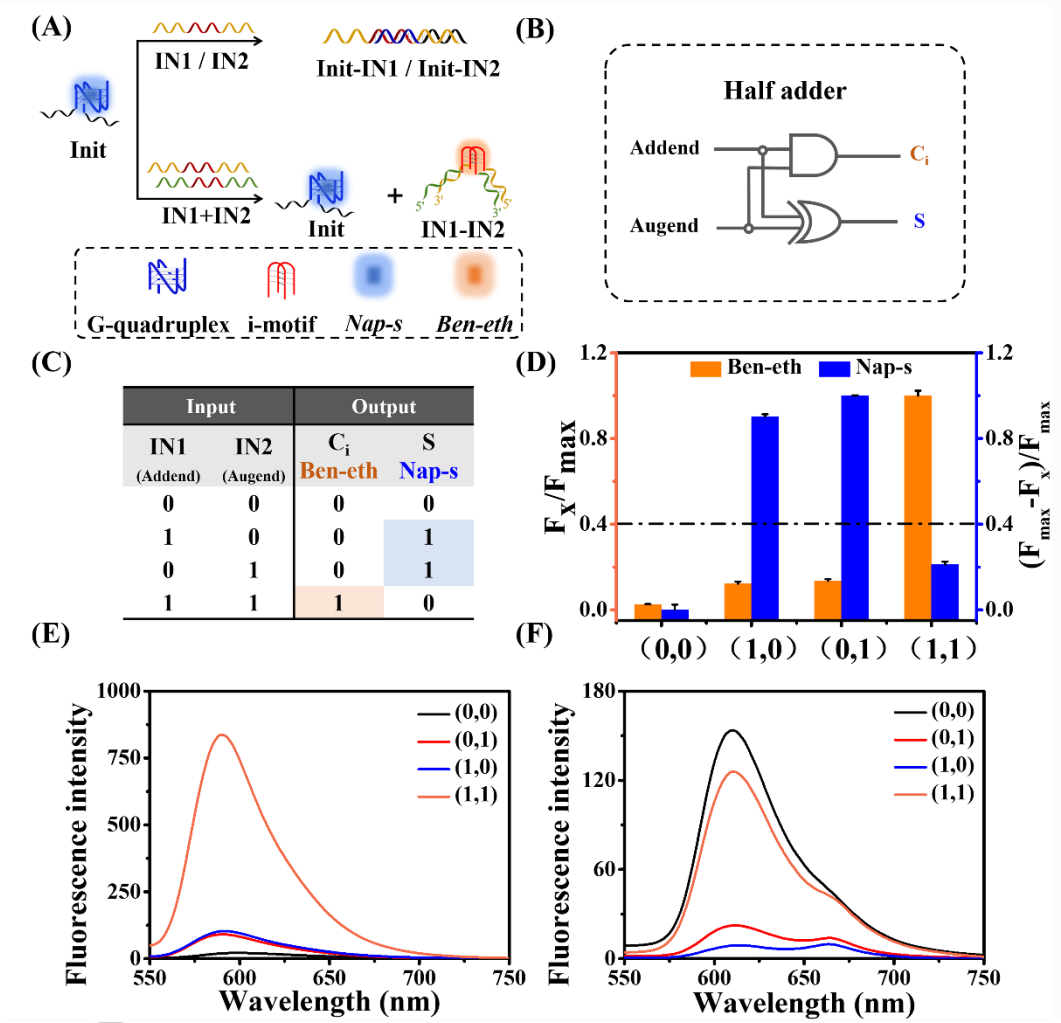

Figure 2. The half adder. (A) The schematic diagram of the half adder based on DNA tetraplex platform. The logic circuit (B) and the truth table (C) of the half adder. (D) The column diagram of the normalized output signals. (E) and (F) show the detailed fluorescence spectra of ***Ben-eth*** and ***Nap-s*** in various input situations, respectively.

10.1002/chem.201900734

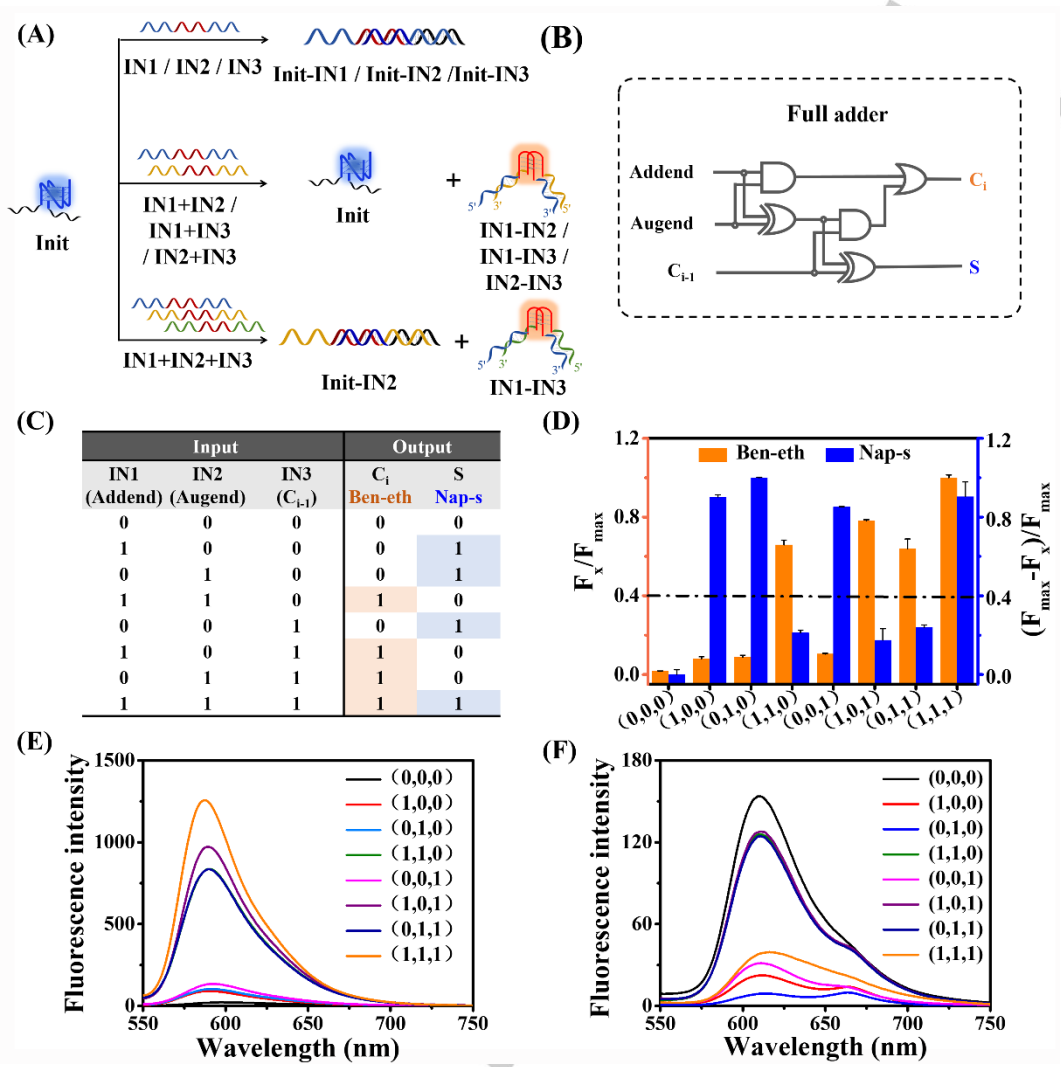

Input			Output	
IN1 (Addend)	IN2 (Augend)	IN3 (C_{i-1})	C_i Ben-eth	S Nap-s
0	0	0	0	0
1	0	0	0	1
0	1	0	0	1
1	1	0	1	0
0	0	1	0	1
1	0	1	1	0
0	1	1	1	0
1	1	1	1	1

Figure 3. The full adder. (A) The schematic diagram of the full adder. The logic circuit (B) and the truth table (C) of the full adder. (D) The histogram of the normalized output signals. (E) and (F) show the detailed fluorescence spectra of ***Ben-eth*** and ***Nap-s*** in various input situations, respectively.

designed in a more straightforward definition. Transfer gate which can transfer the states of inputs to corresponding outputs without cross interference plays key roles in the data transmission and presents broad prospect in environmental monitoring and medical diagnosis.[13c, 22] As shown in Figure 4A, two hairpin strands with C- and G-rich segments, i.e. **Init1*** and **Init2***, were employed as the initial state and two miRNA sequences (*miR 125a* and *miR 184*) were selected as the two inputs (**IN1*** and **IN2***). All the sequences were listed in Table S1. And the normalized fluorescence enhancements (F_x/F_{max}) of the both probes were defined as the outputs O_1 and O_2 (Figure 4B).
leading to the enhancement of the ***Ben-eth*** fluorescence and the quenching of ***Nap-s*** signal, indicating C_i = 1 and S = 1. The normalized outputs were plotted as histogram in Figure 3D, which was consistent with the truth table (Figure 3C) of the full adder. The states and structures of various situations were confirmed by PAGE and CD (Figure S9).

To further demonstrate the scalability of the platform, a full subtractor was also realized by the same strategy with tuned DNA strands [Figure S11-S12, ESI].

The construction of the dual-transfer gate by unified signal definition and the co-analysis on miRNAs

In the aforementioned dual-output logic circuits, the signal definitions are opposite in the ***Ben-eth*** and ***Nap-s*** channels: the high ("light-up") fluorescence intensity of ***Ben-eth*** was assigned as "1", while that of ***Nap-s*** was assigned as "0". To further simplify the processing of output signals, a dual-transfer gate was

10.1002/chem.201900734

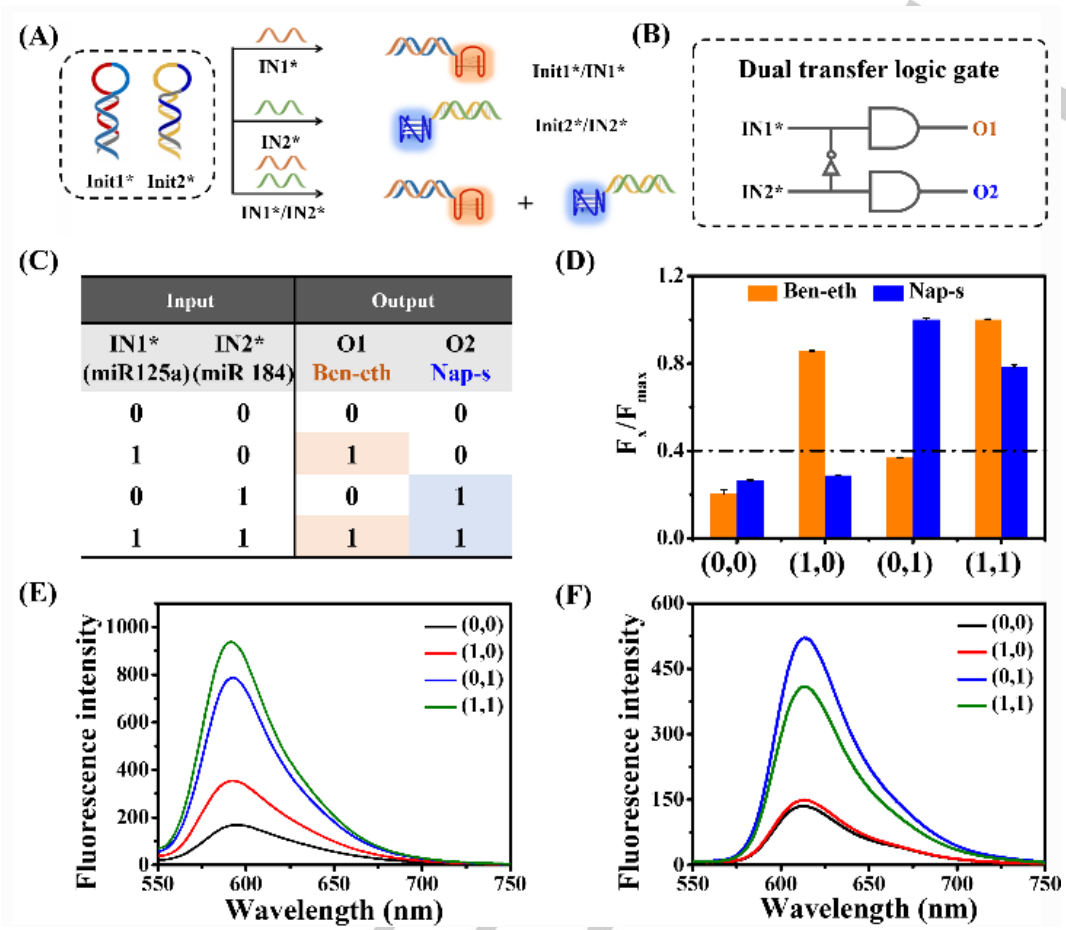

Figure 4. The dual-transfer gate. (A) The schematic diagram of the dual-transfer gate. The logic circuit (B) and the truth table (C) of the dual-transfer gate. (D) The histogram of the normalized output signals. (E) and (F) show the detailed fluorescence spectra of ***Ben-eth*** and ***Nap-s*** in various input situations, respectively.

designed in a more straightforward definition. Transfer gate which can transfer the states of inputs to corresponding outputs without cross interference plays key roles in the data transmission and presents broad prospect in environmental monitoring and medical diagnosis.[13c, 22] As shown in Figure 4A, two hairpin strands with C- and G-rich segments, i.e. **Init1*** and **Init2***, were employed as the initial state and two miRNA sequences (*miR 125a* and *miR 184*) were selected as the two inputs (**IN1*** and **IN2***). All the sequences were listed in Table S1. And the normalized fluorescence enhancements (F_x/F_{max}) of the both probes were defined as the outputs O_1 and O_2 (Figure 4B).

As shown in Figure 4E-F, in the initial state, **Init1*** and **Init2*** were both in hairpin structure with toehold regions, which could respectively hybridize with **IN1*** and **IN2***. The "opened" **Init1*** or **Init2*** would expose C-/G-rich sequences (red/blue region) that formed i-motif/G-quadruplex in PBS, leading to fluorescence enhancement of ***Ben-eth***/***Nap-s***. The normalized outputs were plotted as histogram in Figure 4D, which was consisted with the truth table (Figure 4C) of the dual-transfer gate. The states and structures of the DNA strands in all situations were confirmed by PAGE and CD (Figure S13).

MiRNAs are short oligonucleotides (19–26 bases) that are suggested to be important regulators of various biological functions. Up- or down-regulation of the expression of miRNAs affects some important cellular processes like proliferation, apoptosis and carcinogenesis.[23] Accordingly, co-analysis of miRNAs provide a possible assay for tumor classification and prognosis evaluation in clinical diagnosis.[24] The transfer gate constructed on the tetraplex platform holds great potential to detect miRNAs separately or simultaneously in an intelligent way and is competent for this task very well.

Herein, we applied the platform to co-analyze two specific miRNAs, i.e. *miR 125a* and *miR 184*, which are associated with the development of oral squamous cell carcinoma [25]. The co-analysis of the two miRNA targets shows great potential in the early clinical diagnosis of oral squamous cell carcinoma. As shown in Figure 5, as the concentration of *miR 125a*/*miR 184* increases, the ***Ben-eth***/***Nap-s*** fluorescence is intensified in a

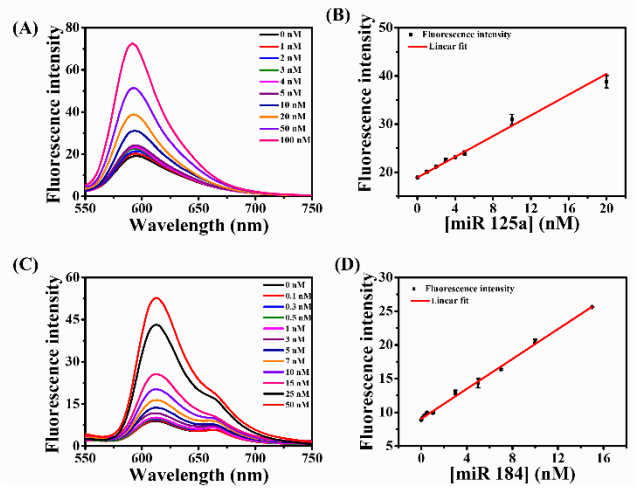

Figure 5. (A) Fluorescence spectra corresponding to the DNA tetraplex platform analyzing different concentrations of *miR 125a* using **IN1*** as a probe. (B) The plots of the fluorescence intensity of ***Ben-eth***. (C) Fluorescence spectra in response to increasing concentrations of the *miR 184*. (D) The plots of the fluorescence intensity of ***Nap-s***. The red lines are fitting curves.

good linear correlation. Following the 3σ criteria, the limits of detecting the both targets were as low as 25 and 19 pM, respectively, which are comparable to the current DNA-based logic sensors.[26] Further, the selectivity of the miRNA sensing was also tested. As shown in Figure S14, several oligonucleotides, including *miR 21*, *miR 122*, *miR 107* and *let 7a*, were selected as the negative control, and none of them exhibits negligible interference on the either detecting channel. The excellent sensitivity and selectively of the miRNA sensor make it potential application in rapid and comprehensive analysis on oncogenic targets.

Furthermore, the biocompatibility is important for a satisfactory logic operation system, so we carried out a further inquiry for that of our designed system. To expand the potential application scenarios of the DNA tetraplexes platform, the Dual-transfer gate was also operated in diluted human serum. As shown in Figure S15, all the results satisfy the logic requirements. The results suggest that the proposed logic platform shows great adaptability for complex biological environments and has potential for clinical diagnosis applications.

Contribution to the design of DNA computation

Different from the digital units that connected by physical wires, DNA circuits are usually functional integrated, which may endow them with great advantages in minimizing the size and accelerate the speed of computation. However, the integrated construction increases the difficulty in design, especially for the advanced logic devices. Take the adder as an example. It is the fundamental and significant arithmetic circuit, but only a few DNA half adders and three full adders have been reported (some works were listed in Table S5), due to the increased computational complexity of the process. And none of the full adder is completely label-free. In this work, by integrating G-quadruplex and i-motif together, we firstly realized a label-free and homogeneous platform that can implement both the full adder and full subtractor functions.

The strategy of integrating the two tetraplex structures in one circuit presents several distinct advantages. First of all, since G- and C-rich sequences can complement with each other, integrating G-quadruplex and i-motif in one circuit can make the best of DNA material and simplify the design of the system, which is beneficial for facilitating the troubleshooting of operations. Compared with the reported platform (Table S5), the DNA tetraplex platform developed in this work realized the most complicated arithmetic and non-arithmetic functions with the simplest composition. Secondly, the strategy presents excellent flexibility and scalability. Three important logic functions, including majority gate, half adder and full adder, constructed in this work share the identical DNA sequences, which can be applied in multifunctional devices and avoid the accumulation of DNA waste. Furthermore, all the circuits were constructed in an easy-to-operate and biocompatible system without enzyme, pre-labelled fluorophores/quenchers, or heterogeneous materials, which provides a potential insight into the fabrication of smart sensory devices that can be adapted to various situations.

Conclusions

In summary, a completely label-free platform was designed through integrating two kinds of DNA tetraplexes, G-quadruplex and i-motif. Three advanced logic operations, the majority gate, half adder and full adder, were realized gradually with identical sequences, which greatly simplify the design of this system. The platform can also be extended to implement the full subtractor function through altering the DNA sequences. In addition, a dual-transfer gate was also constructed with a more straightforward signal definition. Apart from a futuristic vision for molecular computing, the platform can be used as a sensor prototype to co-analysis multiple miRNA targets. Given the excellent versatility, expandability and biocompatibility, more advanced logic devices, such as the demultiplexer and reversible logic gates, are expected to be realized on the same strategy and more applications to be develop in biocomputing, multi-parameter sensing and medical diagnosis.

Experimental Section

Chemicals and instruments

All chemicals (analytical grade) were purchased from Titan technology Co. Ltd. (Shanghai, China) and used without further purification. Synthetic oligonucleotides were purchased from Shanghai Sangon Biotechnology Co. Ltd. (Shanghai, China). ***Ben-eth*** and ***Nap-s*** were synthesized according to the methods of Hamer[27] and Ficken[28], and the purity was determined by MS, elemental analysis, NMR and absorption spectroscopy. (Figure S1-S8 and Table S2-S4) The stock solution of ***Nap-s*** and ***Ben-eth*** was prepared by dissolving its powder in methanol and was stored in darkness. The water was prepared by an ULUPURE (Chengdu, China) ultrapure water system and used throughout the experiments.

Absorption and fluorescent assays

Absorption spectra were acquired with an EVOLUTION 201 spectrophotometer (Thermo SCIENTIFIC, USA) at 25 °C in a 10 mm quartz cell. Fluorescence spectra were collected with an F-4600 spectrophotometer (HORIBA, Japan) in a 10 mm quartz cell at the room temperature, Xenon arc lamp was used in the excitation light source in fluorescence measurement. The excitation wavelength was 530 nm. Both excitation and emission slits were 5 nm, and the voltage was 400 V with a scan speed of 1200 nm/min.

Operation of the logic circuits

Logic gates were assembled using commercial oligonucleotides as described. The DNA stock samples were prepared in pH 7.4 buffer solution (10 mM K_2HPO_4/KH_2PO_4, 100 mM KCl, and 10 mM $MgCl_2$) and stored for more than 24 h at 4 °C. Then the concentrations were estimated by measuring the absorbance at 260 nm. Each sample was prepared by heating at 95 °C for 5 min and then annealed by cooling to room temperature and diluted with PBS (10 mM K_2HPO4/KH_2PO4, 100 mM KCl, 10 mM $MgCl_2$, pH=5.5) before detecting. The final concentration of each DNA strand was 2 μM, while those of **IN1′**, **IN2′** and **IN3′** in the half/full subtractor system were 4 μM. The ***Ben-eth*** and ***Nap-s*** stock solutions (200 μM in methanol) were directly added in the measuring samples and tested after incubating 30 minutes at room temperature in the dark.

Native polyacrylamide gel electrophoresis

Non-denaturing polyacrylamide gel (20%) was prepared in TAE buffer (50 mM Tris, acetic acid, pH 7.0). In each sample, the concentration of each DNA strand was 5 μM. And each sample (20 μL) was mixed with 3 μL Loading Buffer Mix before loading onto the gel. Gel electrophoresis was run in the same buffer at the room temperature for 100 min under a voltage of 100V. The gel was then stained by SYBR-Gold for about 15 min and photographed by Tanon 1600 Gel Imaging System (Shanghai, China).

Circular dichroism spectrum

CD spectra were recorded on a Chirascan Plus spectrophotometer (Applied Photophysics, UK) at room temperature, using a quartz cell of 10 mm optical path length and an instrument scanning speed of 200 nm/min, over a wavelength range of 200–400 nm.

Acknowledgements

This work is supported by the Graduate Student's Research and Innovation Fund of Sichuan University (2018YJSY051). The kind assistance of Prof. Peng Wu and Yani Xie from the Analytical & Testing Centre at Sichuan University with the CD measurements was greatly appreciated.

Conflict of interest

The authors declare no conflict of interest.

Keywords: DNA logic circuit • G-quadruplex• i-motif • label-free • detection

[1] a) D. Margulies, G. Melman and A. Shanzer, *J. Am. Chem. Soc.,* 2006, 128, 4865-4871; b) D. Margulies, G. Melman and A. Shanzer, Nat. Mater., 2005, 4, 768-771; c) D. Margulies, G. Melman, C. E. Felder, R. Arad-Yellin and A. Shanzer, *J. Am. Chem. Soc.,* 2004, 126, 15400-15401.

[2] L. M. Adleman, *Science* 1994, 266, 1021-1024.

[3] a) F. Pu, J. Ren and X. Qu, *Adv. Mater.,* 2014, 26, 5742-5757; b) F. Pu, E. G. Ju, J. S. Ren and X. G. Qu, *Adv. Mat.,* 2014, 26, 1111-1117; c) X. Ran, Z. Z. Wang, E. G. Ju, F. Pu, Y. Q. Song, J. S. Ren and X. G. Qu, *Nanotechnol.,* 2018, 29; d) C. C. Wu, S. Wan, W. J. Hou, L. Q. Zhang, J. H. Xu, C. Cui, Y. Y. Wang, J. Hu and W. H. Tan, *Chem. Commun.,* 2015, 51, 3723-3734.

[4] a) F. A. W. R. Orbach, O. Lioubashevski, R. D. Levine, F. Remacle and I. Willner, *Chem. Sci.,* 2014, 5, 3381-3387; b) H. Y. Lin, J. Z. Chen, H. Y. Li and C. N. Yang, *Sci. Rep.,* 2015, 5, 10686; c) C. Yang, D. Zou, J. Chen, L. Zhang, J. Miao, D. Huang, Y. Du, S. Yang, Q. Yang and Y. Tang, *Chem. Eur. J.,* 2018, 24, 4019-4025.

[5] W. T. Huang, H. Q. Luo and N. B. Li, Anal Chem 2014, 86, 4494-4500.

[6] J. Chen, S. Chen and F. Li, *Anal. Chem.,* 2018, 90, 10311-10317.

[7] a) J. Y. Lu, X. X. Zhang, W. T. Huang, Q. Y. Zhu, X. Z. Ding, L. Q. Xia, H. Q. Luo and N. B. Li, *Anal. Chem.,* 2017, 89, 9734-9741; b) J. Chen, S. Zhou and J. Wen, *Angew. Chem. Int. Ed.,* 2015, 54, 446-450.

[8] W. Li, Y. Yang, H. Yan and Y. Liu, *Nano Lett.,* 2013, 13, 2980-2988.

[9] a) S. Wang, J. Sun, J. H. Zhao, S. S. Lu and X. R. Yang, *Anal. Chem.,* 2018, 90, 3437-3442; b) C. Yang, S. Yang, J. Li, Y. Du, L. Song, D. Huang, J. Chen, Q. Zhou, Q. Yang and Y. Tang, *Anal. Chem.,* 2018, 90, 10585-10590; c) S. Yang, C. Yang, D. Huang, L. Song, J. Chen and Q. Yang, *Chem. Eur. J.,* 2018; d) A. Bader and S. L. Cockroft, *Chem. Eur. J.,* 2018, 24, 4820-4824.

[10] a) J. h. Chen, Pan. J.f. and Chen S, *Chem. Sci.,* 2018, 9, 269-534; b) S. Bi, Y. Yan, S. Hao and S. Zhang, *Angew. Chem. Int. Ed.,* 2010, 49, 4438-4442.

[11] W. T. Huang, J. R. Zhang, W. Y. Xie, Y. Shi, H. Q. Luo and N. B. Li, *Biosens. Bioelectron.,* 2014, 57, 117-124.

[12] H. L. Li, S. J. Guo, Q. H. Liu, L. D. Qin, S. J. Dong, Y. Q. Liu and E. K. Wang, *Adv. Sci.,* 2015, 2, 1500054.

[13] a) R. R. Gao, S. Shi, Y. Zhu, H. L. Huang and T. M. Yao, *Chem. Sci.,* 2016, 7, 1853-1861; b) D. Fan, J. Zhu, Y. Liu, E. Wang and S. Dong, *Nanoscale* 2016, 8, 3834-3840; c) Y. T. M. Gao R.R., Lv X.Ya., Zhu Y.Y., Zhang Y.W. and Shi S, *Chem. Sci.,* 2017, 8, 4139–4668; d) S. Zhang, K. Wang, C. Huang, Z. Li, T. Sun and D. M. Han, *Nanoscale* 2016, 8, 15681-15688.

[14] a) L. Shi, P. Peng, Y. Du and T. Li, *Nucleic Acids Res.,* 2017, 45, 4306-4314; b) T. Li and M. Famulok, *J. Am. Chem. Soc.,* 2013, 135, 1593-1599; c) T. Li, D. Ackermann, A. M. Hall and M. Famulok, *J. Am. Chem. Soc.,* 2012, 134, 3508-3516; d) M. Zeraati, D. B. Langley, P. Schofield, A. L. Moye, R. Rouet, W. E. Hughes, T. M. Bryan, M. E. Dinger and D. Christ, *Nat. Chem.,* 2018, 10, 631-637; e) D. Margulies and A. D. Hamilton, *J. Am. Chem. Soc.,* 2009, 131, 9142-9143; f) Omer Lustgarten, Raanan Carmieli, Leila Motiei and a. D. Margulies, *Angew. Chem. Int. Ed.,* 2019, 58, 184-188.

[15] a) Y. H. Shi, H. X. Sun, J. F. Xiang, H. B. Chen, Q. F. Yang, A. J. Guan, Q. Li, L. J. Yu and Y. L. Tang, *Chem. Commun.,* 2014, 50, 15385-15388; b) J. Zhou, S. Amrane, D. N. Korkut, A. Bourdoncle, H. Z. He, D. L. Ma and J. L. Mergny, *Angew. Chem. Int. Ed.,* 2013, 52, 7742-7746; c) C. Y. Zhou, C. T. Wu, Y. Q. Liu and E. K. Wang, *Rsc Adv.,* 2016, 6, 106641-106647.

[16] C. H. Leung, D. S. Chan, B. Y. Man, C. J. Wang, W. Lam, Y. C. Cheng, W. F. Fong, W. L. Hsiao and D. L. Ma, *Anal. Chem.,* 2011, 83, 463-466.

[17] a) Y. Y. Fan, Z. L. Mou, M. Wang, J. Li, J. Zhang, F. Q. Dang and Z. Q. Zhang, *Anal. Chem.,* 2018, 90, 13708-13713; b) Y. Hu, F. Lin, T. Wu, Y. Zhou, Q. Li, Y. Shao and Z. Xu, *Anal. Chem.,* 2017, 89, 2181-2185.

[18] X. Wei, W. Lin, N. Ma, F. Luo, Z. Lin, L. Guo, B. Qiu and G. Chen, *Chem. Commun.,* 2012, 48, 6184-6186.

[19] a) C. Yang, D. Zou, J. Chen, L. Zhang, J. Miao, D. Huang, Y. Du, S. Yang, Q. Yang and Y. Tang, *Chem. Eur. J.,* 2018, 24, 4019-4025; b) Q. F. Yang,

10.1002/chem.201900734

J. F. Xiang, S. Yang, Q. Li, Q. J. Zhou, A. J. Guan, X. F. Zhang, H. Zhang, Y. L. Tang and G. Z. Xu, *Nucleic Acids Res.,* 2010, 38, 1022-1033.

[20] W. Li, Y. Yang, H. Yan and Y. Liu, *Nano Lett.,* 2013, 13, 2980-2988.

[21] C. Zhou, D. Liu, C. Wu, Y. Liu and E. Wang, *Nanoscale* 2016, 8, 17524-17531.

[22] J. Andréasson, U. Pischel, S. D. Straight, T. A. Moore, A. L. Moore and D. Gust, *J. Am. Chem. Soc.,* 2011, 133, 11641-11648.

[23] J. W. Catto, S. Miah, H. C. Owen, H. Bryant, K. Myers, E. Dudziec, S. Larre, M. Milo, I. Rehman, D. J. Rosario, E. Di Martino, M. A. Knowles, M. Meuth, A. L. Harris and F. C. Hamdy, *Cancer Res.,* 2009, 69, 8472-8481.

[24] a) M. X. Li, W. Zhao, H. Wang, X. L. Li, C. H. Xu, H. Y. Chen and J. J. Xu, *Anal. Chem.,* 2018, 90, 14255-14259; b) S. Lu, S. Wang, J. Zhao, J. Sun and X. Yang, *Anal. Chem.,* 2017, 89, 8429-8436.

[25] W. S. Santhi, R. Prathibha, S. Charles, K. G. Anurup, G. Reshmi, S. Ramachandran, V. T. Jissa, P. Sebastian and M. Radhakrishna Pillai, *Oral Oncol.,* 2013, 49, 567-575.

[26] J. K. Deng, Z. H. Tao, Y. Q. Liu, X. D. Lin, P. C. Qian, Y. L. Lyu, Y. F. Li, K. Fua and S. Wang, *Chem. Commun.,* 2018, 54, 3110-3113.

[27] Hamer, F.M. The Chemistry of Heterocyclic Com-pounds, Interscience, New York, **1964**).

[28] Ficken, G.E. The Chemistry of Synthetic Dyes, (Aca-demic Press, New York, 1971).M. Prudent and H. H. Girault, *Metallomics* **2009**, *1*, 157-165.

10.1002/chem.201900734

WILEY-VCH

Entry for the Table of Contents

FULL PAPER

By integrating two DNA tetraplexes, G-quadruplex and i-motif, a versatile and completely label-free platform is established, on which a series of arithmetic and nonarithmetic logic functions are implemented, including the half/full adder, full subtractor, majority gate and dual-transfer gate. Among them, the dual transfer gate is applied to analyse two important micro-RNA biomarkers (*miR 125a* and *miR 184*).

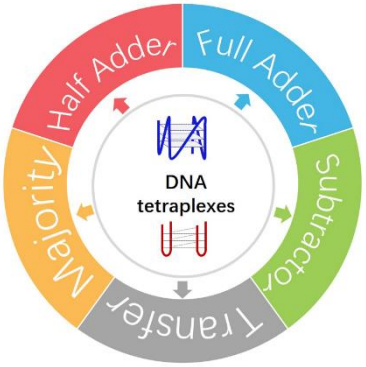

D. Huang, C. R. Yang, Y. Yao, J. C. Li, C. Guo, J. C. Chen, Y. Zhang, S. Yang, Q. F. Yang,* Y. L Tang

Page No. – Page No.

Versatile and homogeneous DNA tetraplex platform for constructing label-free logic devices: from design to application